

Research Article

Surface, optical and electrochemical performance of indium-doped ZnO/WO_3 nano-composite thin films

Reza Mohammadigharehbagh[1,2] · Suat Pat[1] · Nihan Akkurt[1] · Ali Olkun[3] · Mustafa Ozgur[1] · Uğur Demirkol[1] · Soner Özen[4] · Şadan Korkmaz[1]

Received: 5 April 2020 / Accepted: 22 September 2020
© Springer Nature Switzerland AG 2020

Abstract
Great demand on replacing emission and pollution-free materials for energy storage by traditional fossil fuels has led to investigating of high-performance electrochromic materials. Nano-composite for electrochromic device may be a good choice. In this paper, stack-structured indium-doped ZnO/WO_3 nano-composite thin films were deposited on glass, indium-doped tin oxide (ITO) and fluorine-doped tin oxide (FTO)-coated glass substrates, respectively. Surface, optical and electrochromic (EC) performance of the prepared nano-composite films has been investigated. Electrochromic impedance spectroscopy (EIS), cyclic voltammetry, repeating chronoamperometry (CA) and chronocoulometry (CC) measurements were taken. The Raman spectroscopy measurement shows that high-intensity peaks are related to ZnO wurtzite structure for all substrates. In the CA measurement, the rate of Li^+ transfer between surface and electrolyte was faster for films coated onto ITO substrate. In addition, the intercalation/deintercalation of Li^+ was obviously found faster for films onto ITO substrate due to roughness, structure differences than the other sample. As an advantage of our nano-composite material, the absence of current decay in the both coloration and bleaching stages has proved superiority and stability of films as well as indium contribution. The reversibility of stack-structured $InZnO/WO_3$ nano-composite films was computed as 30 and 50% for the film with ITO and FTO substrates. The highest coloration efficiency value has calculated as 80 and 69 cm^2/C for nano-composite thin films deposited onto FTO substrate @ 632 and 550 nm, respectively. Warburg impedance element values were determined from the equivalent circuit model. Also, calculated charges were determined for bleaching or coloring process for all films.

Keywords In-doped ZnO/WO_3 nano-composite · Electrochromic performance · Surface properties · Coloration efficiency

1 Introduction

In our technological and modern world, using of cutting edge materials instead of fossil fuels has attracted great deals due to decreasing pollution and emission, achieving economical energy as well as low power consumption in our life [1]. In this way, various types of semiconductor compounds such as ZnO, WO_3, Fe_2O_3, TiO_2 and others are under consideration through researchers owing to their outstanding properties [2]. ZnO has been an extensively investigated. Though TiO_2 is widely and frequently employed owing to their own significant capability, ZnO is well alternative candidate [3]. The optical band values of pristine ZnO are commonly reported as 3.37 eV [4].

Electrochemical (EC) characteristics of the produced nano-structured thin films are still taking into account.

✉ Suat Pat, suatpat@ogu.edu.tr | [1]Department of Physics, Eskişehir Osmangazi University, Eskişehir 26480, Turkey. [2]Department of Physics, Urmia Branch, Islamic Azad University, Urmia, Iran. [3]Physics Department, Bursa Uludağ University, Bursa, Turkey. [4]Bozok University, Yozgat, Turkey.

SN Applied Sciences (2020) 2:1780 | https://doi.org/10.1007/s42452-020-03580-7

Published online: 06 October 2020

Since using the thin films in diverse fields of applications, different nanostructured metal oxides, WO_3, V_2O_5, TiO_2 and NiO are extensively investigated in recent years [5] [6]. Owing to privilege and significant contribution to industries as well as optical band gap (~ 2.35–3.27 eV), then WO_3 has been selected as conductive layer [7]. According to the literature, ZnO and WO_3 thin films were deposited via sputtering, chemical vapor deposition, sol-gel, evaporation and spray pyrolysis techniques [8–11].

In this study, stack-structured nano-composite indium-doped ZnO/WO_3 thin films are deposited onto un-coated glass, indium-doped tin oxide (ITO) and fluorine-doped tin oxide (FTO)-coated glass substrates. These nanostructured composite thin films have carried out by thermionic vacuum arc technique. Then, structural, optical and electrochemical properties have been investigated by atomic force microscopy, field emission scanning electron microscopy, Raman spectroscopy and UV–Vis spectrophotometry and potentiostat/galvanostat. Detail electrochemical performance of the prepared thin films is comprehensively investigated using electrochemical impedance spectroscopy, cyclic voltammetry, repeated and chronoamperometry, chronocoulometry and iono-optical studies. The main motivation of this investigation is to obtain improved electrochromic performance use with a stack-structured nano-composite InZnO/WO_3.

2 Experimental detail

A thermionic vacuum arc (TVA) technique has been chosen as coating system of the nano-composite thin film deposition. This technique is working on high vacuum regime, relying upon plasma technology. A TVA system has four different parts, that is, vacuum pumps and vessels, electronic measurement components (such as voltmeter and ampere meter), electrodes systems (such as substrate holder, cathode, anode and crucible) and finally pressure gauges.

The substrates were carefully cleaned by deionized water and after that ethylene continuously for removing any residual contamination. On the other hand, the desired materials mean WO_3 has pressed to pellet form and then takes place in molybdenum crucible as first route. The vacuum chamber was vacuumed to 5×10^{-5} torr. WO_3 thin films were deposited onto indium tin oxide (ITO) and fluorine tin oxide (FTO)-coated glass substrate and un-coated glass substrate.

In the second route, indium and ZnO powders were pressed to pellet form and then placed in the evaporation boat. The overall procedure is executing in the same situation. Indium-doped ZnO thin film was deposited onto WO_3 thin film-coated, un-coated, ITO and FTO-coated glass substrate. All substrates are kept in the same situations for each experiment. The TVA deposition parameters during the first and second route are summarized in Table 1.

3 Results and discussion

The morphological properties of the prepared thin films have been carried out using atomic force microscopy (AFM). An Ambios Q-scope AFM with scan atomic V 5.1.0 SPM software was used for the surface measurements. All measurements were taken place in room temperature at non-contact mode by applying of 6-Hz scan rate. Using AFM measurement the main and significant morphological parameters such as root-mean-square (RMS) roughness, skewness (Ssk), kurtosis (Skr) and peak–valley values of the produced thin films have obtained. The obtained results are depicted in Table 2.

According to the AFM results from Fig. 1a–c, the minimum and maximum root-mean-square (RMS) roughness values of the coated In-doped ZnO/WO_3 thin films were

Table 2 Surface properties values of the deposited nano-composite films

Samples	RMS (nm)	Skewness (Ssk)	Kurtosis (Skr)
InZnO/WO_3/un-coated glass	1.54	0.94	3.21
InZnO/WO_3/ITO-coated glass	3.33	1.69	4.33
InZnO/WO_3/FTO-coated glass	17.29	0.5	-0.1

Table 1 Deposition parameters for stack-structured nano-composite

Deposition sample	Discharge current	Applied voltage	Filament current	Working pressure	Base pressure	Deposition time
Unit	A	V	A	torr	torr	min
WO_3	0.08	350 → 350	22	2×10^{-4}	8×10^{-5}	7
In-doped ZnO	0.6	800 → 0	20.7	1×10^{-4}	8×10^{-5}	2

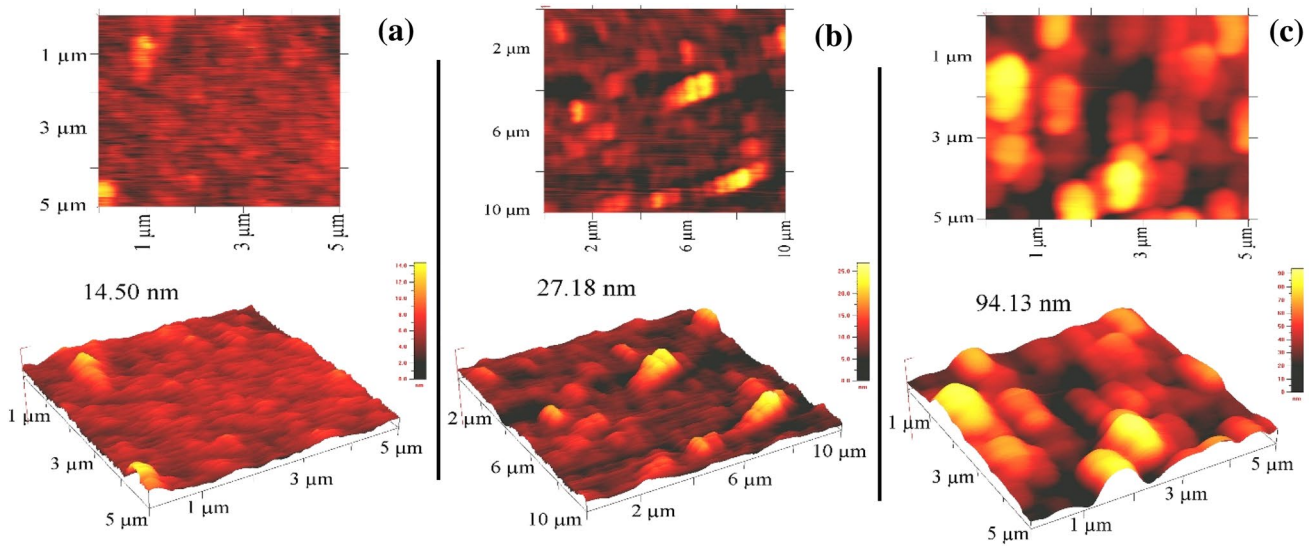


Fig. 1 Two- and three-dimensional AFM images of the nano-composite thin films deposited on **a** un-coated glass, **b** ITO-coated and **c** FTO-coated glass substrates. Images were taken from the top In-doped ZnO layer

observed onto the FTO and un-coated glass substrates, respectively. The obtained data clearly demonstrated that InZnO/WO_3 onto glass substrate is smoother than the films deposited on other samples notably; in all 3 substrates, deposition of indium-doped ZnO onto WO_3-coated samples has larger grain sizes than the other. The obtained RMS values are interestingly significant in charge transfer capacity, and it is a key characteristic for the materials utilized in optical and electrochemical area [10].

Using AFM, the skewness (Ssk) and kurtosis (Skr) values of the nano-composite films were determined. A Ssk value has revealed shape of the surface distribution as well as indication of symmetry of variations occurs on a films surface. This parameter is originating from deep valleys or high peaks appearing on the surface of produced films. Skr value is related to the distribution of the spike likes growth after coating of thin films above and below the average line defined by the device is specified. On another insight, the value also is demonstration of surface flatness.

Field emission scanning electron microscopy (FESEM) images of InZnO/WO_3 nano-composite thin films have been carried out at 50 Kx magnification using Carl Zeiss Supra 55 model instrument. Obtained images are shown in Fig. 2a–c. According to Fig. 1a–c, the composite deposited onto the uncoated glass substrate is smoother than the other deposited films onto ITO and FTO-coated glass substrate. The RMS values given in Table 2 are obtained from an AFM device. So, RMS roughness in AFM is related to the grains and agglomerate of the grains. Finally, we found the lowest roughness in Fig. 1a. Obtained results in Table 2 confirm the AFM images. AFM devices cannot detect the narrow cracks, and this is the major disadvantage of the AFM analysis. This disadvantage will eliminate in near future. The cracks and small grains increase the surface area of the film. The cracks in Fig. 1c are bigger than the cracks in Fig. 1a. This is the desired properties of the ion storage applications because ion intercalation/deintercalation is very easy compared to the compact or

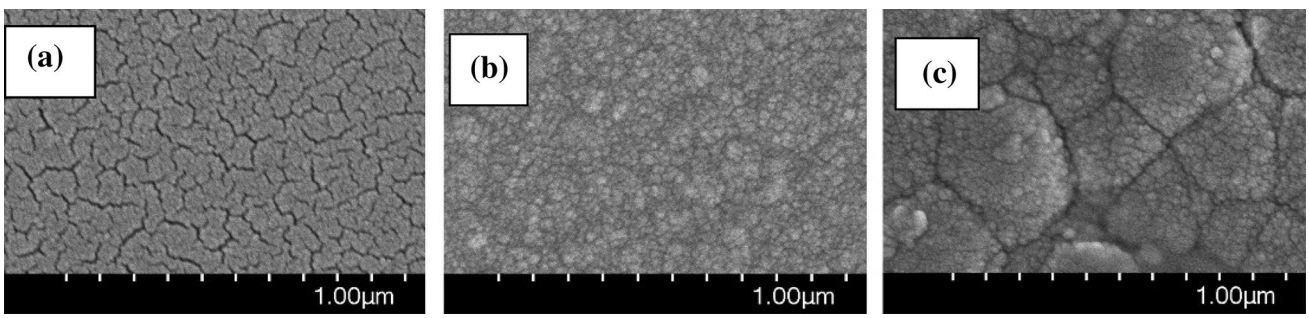


Fig. 2 FESEM analyses images of the prepared nano-composite thin films on **a** un-coated, **b** ITO-coated and **c** FTO-coated glass substrates

hard structure thin films. For imaging of the cracks, FESEM images are a good choice. FESEM images are illustrated in Fig. 1c, and the cracks are shown in Fig. 1a and c. Thus, it can be seen that ion intercalation/deintercalation significantly increases compared with the crack-free films (see in Fig. 6a). The crack in FESEM images (Fig. 2a-c) cannot be seen by AFM measurements. Because AFM images measure only surface topography, the grains or crystallites have a lot of atom and chemical bond. According to the FESEM images, cracks were formed by small grains and crystallites. In particular in Fig. 2a and c, Li^+ ions can reach to atoms located in sub-surfaces. So, the film with crack structure can show the better electrochemical performance according to the surface without cracks. These were proved by obtained data.

The optical band gap (E_g) calculation of the nano-composite films has studied and relied on Tauc method. This method is determined using absorption spectra of the samples obtained by UV–Vis spectrophotometer (Unico Dual Beam 4802) between 1.2 and 4 eV. The E_g values obey the following equation:

$$(\alpha h\nu)^n = A\left(h\nu - E_g\right) \quad (1)$$

Here in, α is absorption coefficient, $h\upsilon$ is the photon energy, and A is a constant. In this equation, $\alpha = 2.303$ (absorption/thickness) and n, which is well known as transition features of the materials. It is worthwhile noting that the thickness values of the thin films were found 110, 150 and 200 nm onto un-coated, ITO-coated and FTO-coated glass substrates via Filmetrics F20 tool. In our case, according to the allowed indirect transition of the ZnO, the $(\alpha h\upsilon)^2$ versus incident photon energy curves are illustrated in Fig. 3. Simply, linear extrapolation of y-axis when cutting energy value is given the optical band gap of the specimens. Thus, the obtained E_g of the In-doped ZnO/WO_3 is lower than the bulk ZnO (3.37 eV) material. The band gaps of the used materials are 3.30–3.48, 2.60–3.00, 3.40–3.80 and 3.86 eV for IZO, WO_3, ITO and FTO layers, respectively. Also, W-doped ZnO layers have a band gap of 3.26 eV. According to Fig. 3, nano-composites have strongly absorption in the range of 1.2–3.6 eV. As can be seen in Fig. 3, optical band gap graphs give indirect band gap for the band deformations. IZO and WO_3 band gaps calculations are seen in the range of 3.30–3.48 eV and 2.60–3.00 eV depicted in Fig. 3, respectively. The values are in a well agreement with reference Girtan [13], Kim [14]. The decrease in the optical band gap values of In-doped ZnO/WO_3 thin films is attributed to diverse factors. These factors are summarized by the crystalline structure, concentration of impurities, types of defects and granular structure of the prepared thin films. According to the literature survey, reduction in the E_g values is inversely implying to indium concentration increment which are in a well harmony of the reported works [15, 16].

The room-temperature photoluminescence (PL) spectroscopy measurement has been taken via PerkinElmer LS-55 at 300-nm excitation wavelength in the range of 350–530 nm. These measurements curves for all prepared films are rendered in Fig. 4. In the case of films deposited on un-coated glass substrate, the high-intensity peaks at 420, 476, 369 and 466 nm in terms of peaks intensity are clearly detectable. The peak at 420 nm (2.96 eV) is indication of violet emission that owing to interface of grain boundaries of indium and zinc oxide grains [17]. The peaks appeared at 476 (2.61 eV), 369 (3.37 eV) and

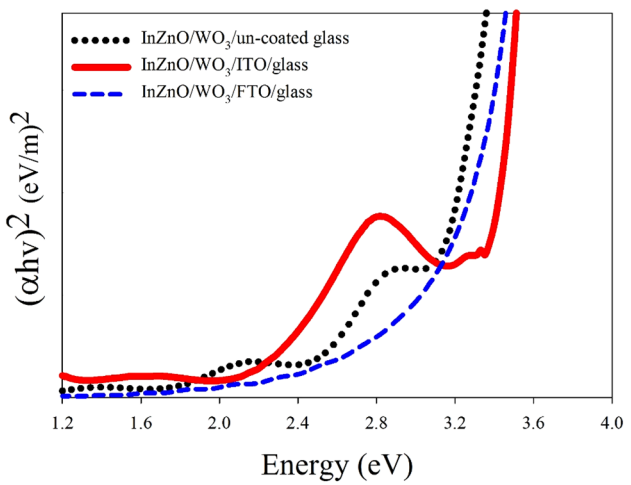


Fig. 3 Optical band gap graphs of InZnO/WO_3 nano-composites thin films onto un-coated, ITO- and FTO-coated glass substrates

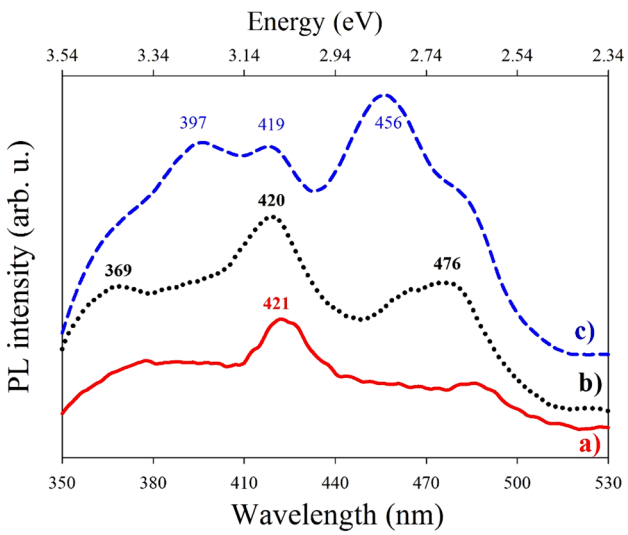


Fig. 4 PL spectra of the nano-composite thin films deposited upon **a** ITO-coated, **b** un-coated glass and **c** FTO-coated glass substrates

466 nm (2.66 eV) are transition of conductance band to oxygen vacancies [18], bound exciton recombination [19] and a blue emission that served as oxygen vacancies [20] of nano-composite thin film. In addition, the low-intensity peak recorded at 521 nm (2.38 eV) is so-called green emission directly attributed to recombination of e^- and h^+ of single oxygen vacancies generated by photo [21].

For the films on ITO substrates, in order to intensity, the peaks at 421, 378, 389, 393, 400 and 409 nm are appeared. The band-to-band absorption in the In-doped ZnO has proved existence of energy transfer between ZnO and indium [22] by peaks marked as 378 nm (3.28 eV) [23]. The case of peaks at 400 (3.1 eV) [24] and 409 nm (3.03 eV) [25] maybe originates from zinc vacancies as well as transitions between conduction band and Zn vacancies as acceptor levels in this structure. Based on results, some weak intensity peaks are also observed at 444, 468, 481 and 491 nm in the measured spectra. The blue emission peaks at 444 and 468 nm are exhibited transition of e^- from shallow donor level to valence band [26] and oxygen vacancies [27]. The decrease in the intensity of these 2 peaks simultaneously causes to decrease oxygen vacancies. Finally, the peaks at 481 nm (2.58 eV) and 491 nm (2.53 eV) inferred as green emission [28] and intensity alleviation means scarcity of antisite oxygen along or Zn vacancies introduced in this structure as well as blue emission [29].

In the InZnO/WO_3 coated on FTO substrates, the 3 strong peaks become manifested at 456, 397 and 419 nm in the given spectra. The peak emerged at 456 nm (2.72 eV) has occurred in valence band by filling h^+ in doubly ionized zinc vacancy sites e^-. These electrons are generated through radiative recombination [18]. Furthermore, 2 weak yellow band peaks that centered at 519 and 523 nm are mainly indicating defect structure emission of produced thin films. Actually, these peaks might be account for oxygen interstitial and oxygen vacancy [30].

Raman spectrum of the prepared In-doped ZnO/WO_3 onto un-coated, ITO-coated and FTO-coated glass substrates is illustrated in Fig. 5. Regarding this figure, in the films deposited on glass substrate, totally 8 main peaks which centered at 1100, 560, 802, 130, 450, 941, 398 and 663 cm^{-1} have emerged in order to intensity amount. The peaks appealed at 1100, 560, 130, 398 and 663 cm^{-1} have allocated to different statuses of ZnO. Thus, those peaks mainly have been shown acoustic combination of A_1 and E_2 [31], the A_1(LO) [32], zone boundary transverse acoustic mode [33], A_1(TO), second-order mode or multiphonon process [33], respectively. Besides, the remaining peaks, i.e., 802 and 450 cm^{-1} at the given spectra, imply υ (O–W–O) [34] and crystalline of monoclinic WO_3 [35], respectively. The peaks also seen at 941 cm^{-1} attributed to WO_6 in this composite structure [36].

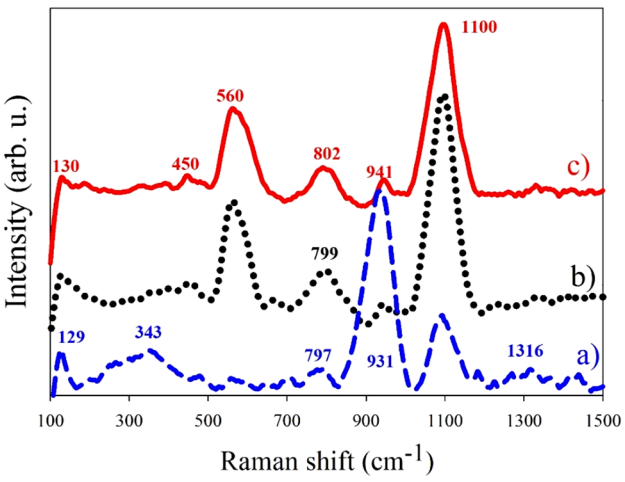


Fig. 5 Raman spectra of the nano-composite thin films deposited on **a** FTO-coated, **b** un-coated and **c** ITO-coated glass substrates

In the case of films coated on ITO substrate, the robust peaks are 1100, 559, 799, 130 and low-intensity peaks also are listed as 945, 450, 398 and 334 cm^{-1}, respectively. The existence of high-intensity peaks is as same as films deposited upon glass substrate. As can be seen, a shift observed at the third main peaks thereby gives rise of indium introducing defect or tensile strain reported by other researchers [37]. For other low-intensity peaks, in terms of intensity the peaks implication of W=O terminal stretching and second-order characteristic are owing to multiphonon procedure, $E_2^{high} - E_2^{low}$ [38]. The remaining peaks were well matched by films coated on glass substrate and introduced in the aforementioned section for films deposited on FTO substrates, and the high- and low-intensity peaks are given as 931, 1100, 129, 343, 266, 797 cm^{-1} and 776, 1182, 558, 586, 202, 707, 482 cm^{-1}. The severe peaks at 931, 343, 266 cm^{-1} contributed to multiphoton scattering in ZnO [39], $ZnWO_4$ formation [40], irregularities of Raman scattering in the B_{1L} mode of ZnO [41], respectively. The peaks exist at 292, 1182, 1316 cm^{-1} specified as unknown, thereby suggesting to belong to other phases of ZnO structures. At the low-intensity peaks, the values such as 776, 586, 202, 707 and 482 cm^{-1} are, respectively, assigned to υ (O–W–O) [34], E_1 low of ZnO [42], second-order modes or multiphonon process and lattice modes (ZnO), monoclinic WO_3 and 2LA by multiphonon process [43], respectively. Based on results, no Raman peak exists in the given spectra that belong to indium or related compounds, demonstrating lack of in-associated secondary phases.

The electrochemical performance of the prepared nano-composite thin films has carried out using Gamry 3000 potentiostat/galvanostat. Electrochemical impedance spectrum (EIS), cyclic voltammetry (CV),

chronoamperometry (CA), repeating chronoamperometry (RCA) and chronocoulometry (CC) measurements have been taken. In all measurements, the 3-electrode arrangements, i.e., working, reference, counter electrode and electrolyte, were selected as In-doped ZnO/WO_3 thin films onto ITO- and FTO-coated glass substrates, Ag/AgCl, ITO-coated glass and 0.1 M $LiClO_4$: propylene carbonate, respectively. The distance between electrodes is kept constant during the measurements. EIS measurements were taken in the range of 10 kHz–0.1 Hz at 10 mV/s. The EIS measurement results of the produced In-doped ZnO/WO_3 thin films using TVA technique are depicted in Fig. 6a and 6b. This analysis usually utilized for better studying and understanding the interfacial charge transfer procedure. According to the plots, it is clearly seen that the films deposited on the ITO-coated substrates show higher resistance with regard to FTO-coated substrate. Indeed, the high- and low-frequency zones are indication of charge transfer and Warburg diffusion impedance and thus include diffusion of ions into the produced composites thin films. In the films deposited onto the ITO-coated substrate, at the high frequencies, the semicircle is not clearly observed due to the control step which already reported by Xie et al. [44]. This semicircle has obviously recognizable in the films onto FTO-coated substrate. It was noticed that in the redox reaction the larger diameter of semicircle is dependent on higher charge transfer resistance happened between film and used electrolyte [45] and vice versa. To this end, in the case of composite thin films deposited onto FTO-coated substrate, the resistance value is lower compared to counterpart. According to obtained data, the cells show different electrochemical behaviors.

The impedance data are useful for deeper discussion for the cell properties. In particular, Warburg impedance element is important for the ion transfer. In Table 3, the values of elements of the equivalent circuit are shown. All obtained values for nano-composites are very close to each other. The values of Warburg elements for circuit are 3.6×10^{-5} and 2.17×10^{-5} Ohmxs$^{-0.5}$ for the cell with

Table 3 Equivalent circuit model and element value

	Cell with ITO	Cell with FTO	Unit
R1	336	354	Ohm
C1	8×10^{-7}	2.6×10^{-7}	Farad
R2	3.2×10^{4}	3.1×10^{4}	Ohm
C3	2.6×10^{-5}	3.6×10^{-5}	Farad
R3	0.17	0.40	Ohm
W3	3.6×10^{-5}	2.17×10^{-5}	Ohmxs$^{-0.5}$
GoF	7.32×10^{-3}	4.74×10^{-3}	

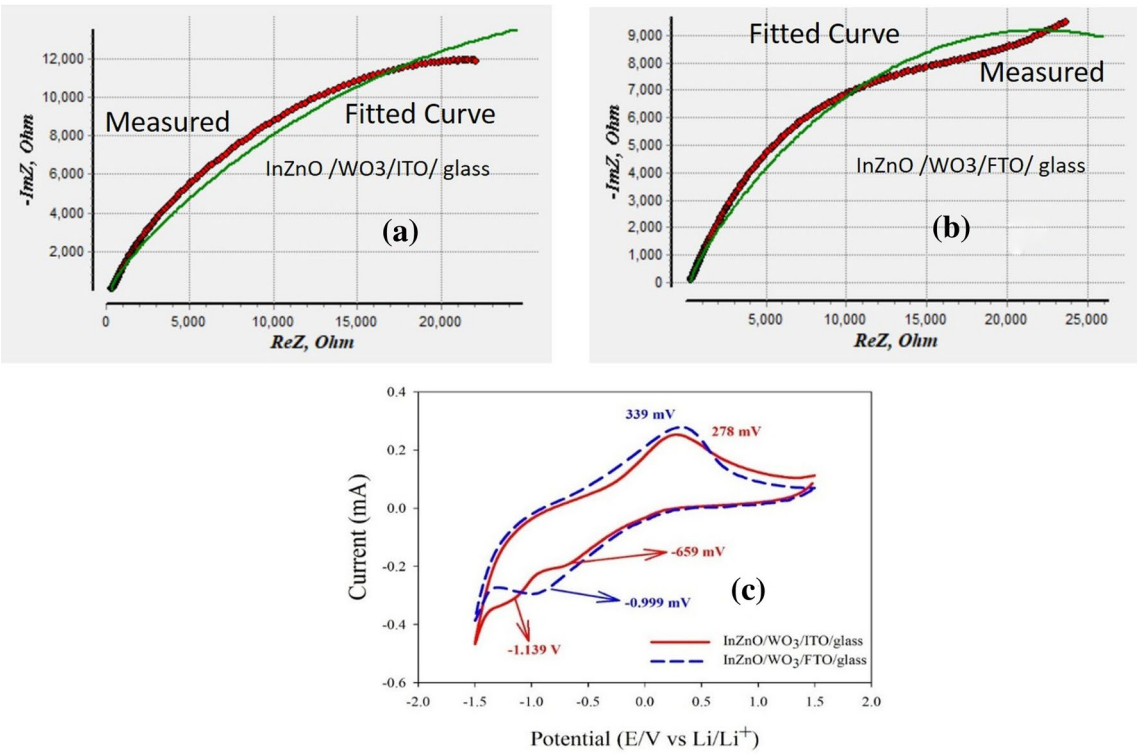
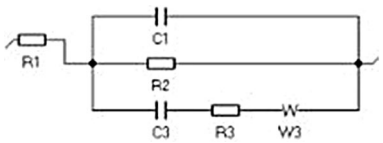


Fig. 6 Nyquist curves of the nano-composite thin films deposited on **a** ITO-coated and **b** FTO-coated glass substrates. **c** Cyclic voltammetry curves of the deposited thin films

ITO or FTO, respectively. The cyclic voltammetry measurement of the film using TVA technique is conducted on ITO-coated and FTO-coated glass substrates. For each substrate, all measurements were taken between ± 1.5 V potential range, scan rate of 10 mV/s and step size of 20 mV at room temperature. Using this technique, the ion insertion/extraction, cathodic and anodic characterization of the nano-composite thin films were investigated and are shown in Fig. 6c.



As can be seen from Fig. 6c, one main cathodic and anodic peaks were emerged in films coated onto FTO-coated glass substrate, while in anodic peak case, the similar condition is not occurring for films coated onto ITO-coated glass substrate. By keeping same scan rate, the cathodic peak values are found as 278 mV and 339 mV for composite films produced onto ITO- and FTO-coated glass substrates. In a same manner, the corresponding current values for same composite films are ordered as 25.32 and 27.86 mA. By taking into account of similar scan rate a shift in the cathodic peak values of the 2 samples revealed. In the anodic region, 2 different peaks at −659 mV and −1.139 V with current values of 18.99 and 30.70 mA for composite films coated onto ITO-coated glass substrate, while only one broad peak centered at −0.999 V with 29.52 mA current value, respectively, has emerged and is plotted in Fig. 6b. The repeated chronoamperometry (RCA) and chronoamperometry (CA) measurement of the In-doped ZnO/WO_3 on ITO- and FTO-coated glass substrates has been taken at the applied potential of +1.2 and −0.5 V as well as +1.5 and −0.5 V ranges in 3 electrode arrangement, respectively. Simply and effectively, the amount of Li^+ insertion and extracted, reversibility and coloration efficiency (CE) performance deduced by this analysis. The In-doped ZnO/WO_3 thin films onto ITO- and FTO-coated glass substrates, which is mounted as working electrode initially, has started as positive value and then stepped to negative value. Meanwhile, the time parameter during the colored to bleached status change registered. The applied current versus time interval is plotted in Fig. 7a and b. The switching kinetics for 2 designed cell is distinctly different. The time duration changes from bleaching to coloration (i.e., insertion of Li ions) states of the films can be easily seen from these Fig. 7a and b. This parameter mainly shows capability of coated films for application in EC used devices. First 10 cycles are very stable for all designed test cell. Generally, electrochromic performance in 10 cycles can change drastically and it strongly depends on the thin film properties such as surface, optical and chemical properties.

It can be clearly realized for films deposited onto FTO-coated glass substrates, and the insertion of Li ions (bleaching) time amount is more than ITO-coated substrates. On the other aspect, in the coloring stage (0–100 s), the rate of Li ion transfers between nano-composites thin films and electrolyte was faster for films coated onto ITO-coated substrates. Similarly, in the bleaching state also the same behavior can be demonstrated for charge-transferring status. It was noticed that the higher bleaching current value is witnessing of good conductivity, though quick increase or decrease in current amount is responsible to conductor to insulator transition. Thus, this transition in the case of In-doped ZnO/WO_3 onto ITO-coated substrate has taken rapidly. In the coloration

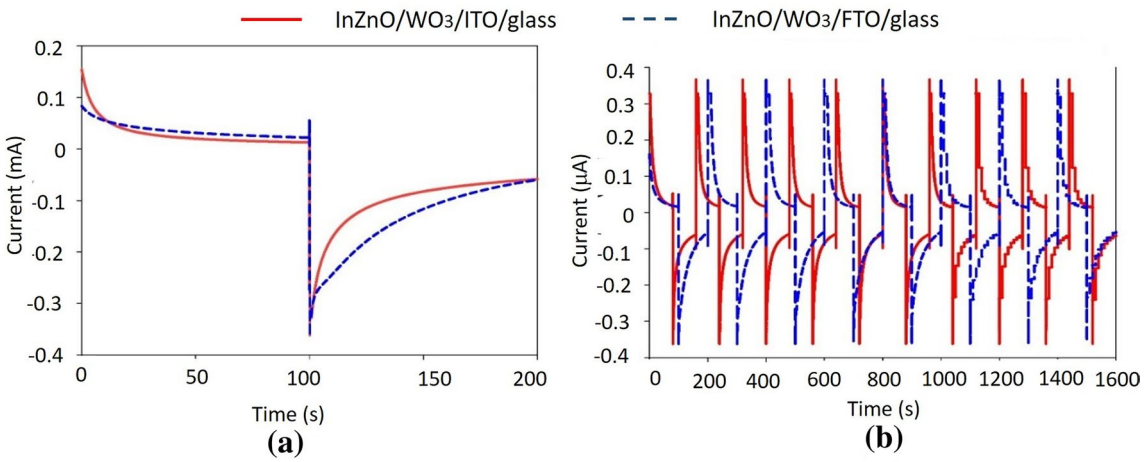


Fig. 7 **a** Chronoamperometry and **b** repeated chronoamperometry plots of InZnO/WO_3 thin films

stage that indication of insulator to conductor transition, the nano-composite films deposited onto ITO-coated glass substrates have shown fast rate decrease compared to counterparts again. This behavior might be attributed to structural, indium contribution and types of substrate differences of the nano-composite thin films by taking same coating conditions. As Fig. 7a shows, the intensity of coloration current for nano-composite films onto ITO-coated glass substrates is more than counterparts. The bleaching intensity as current value view is nearly the same. The time between 0–100 s and 100–200 s was inferred the coloring and bleaching reactions. Overall coloring and bleaching times were recorded as 200 s. Indeed, the color change mechanism time duration ascribed as conductivity of the prepared films and intercalated/deintercalation ion rates. The RCA measurement has also taken for In-doped ZnO/WO_3 nano-composites thin films coated onto both ITO- and FTO-coated glass substrates in 10 cycles. Taking into consideration the time duration of nano-composite film prepared onto ITO-coated glass substrate is faster that indicates quick transition and conductivity in order to time progress. Besides this, lack of decay in the intensity of coloration and bleaching mechanism has mainly proved superiority and stability of the prepared nano-composite films manufactured by TVA technique.

The Li^+ ion insertion and extraction procedure in order to time variation was carried out for In-doped ZnO/WO_3 nano-composite thin films on both ITO- and FTO-coated glass substrates. The analyses were done by applying voltage as −0.5 to1 V and −0.5 to 1.2 V for films coated onto ITO- and FTO-coated glass substrates at room temperature, respectively. Utilizing the results given by this analysis (Fig. 8a), the reversibility of the nano-composite films is calculated by obeying the following equation:

$$\text{Re}versibility = {}^{Q_{\text{din}}}/_{Q_{\text{in}}} \quad (2)$$

where the de-intercalation (Q_{din}; coloration) to intercalation ($Q_{\text{in;}}$ bleaching) charge amount after given time is represented as reversibility value. The reversibility of the In-doped ZnO/WO_3 nano-composite thin films was 30 and 50% onto the ITO- and FTO-coated glass substrates, respectively.

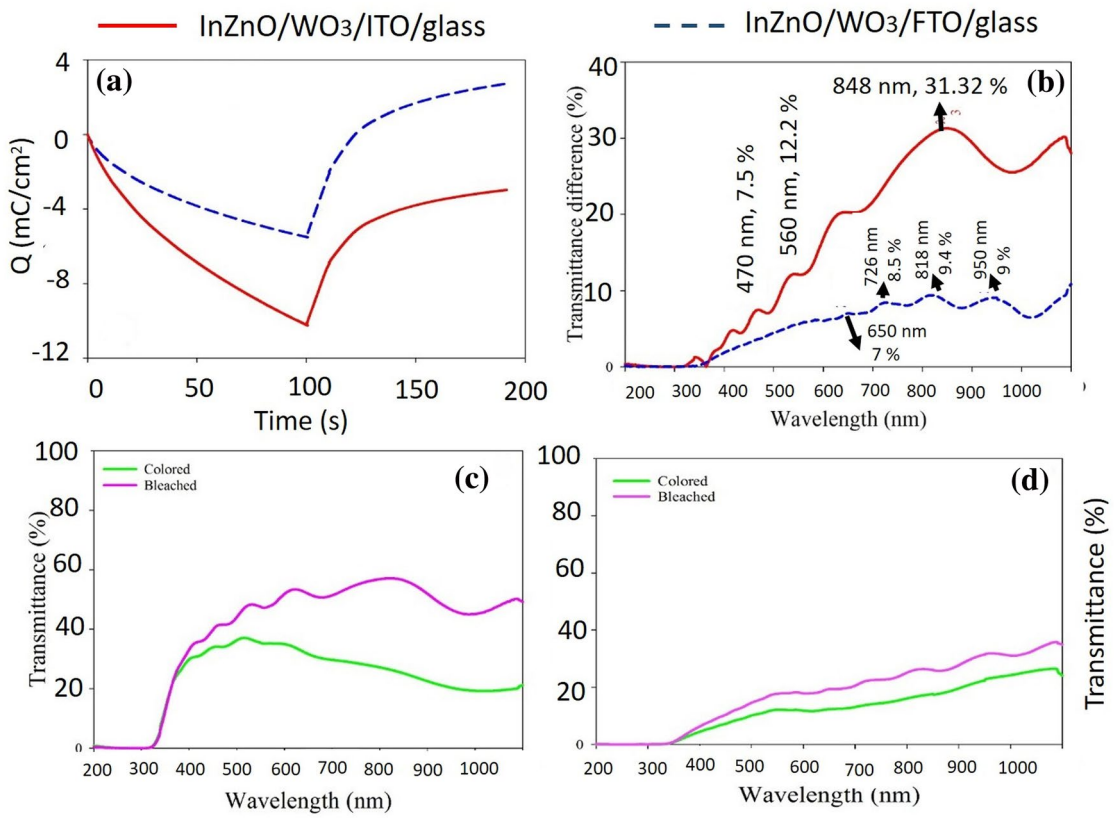


Fig. 8 **a** Chronocoulometric profiles, **b** optical transmittance differences spectra and **c**, **d** colored and bleached status of InZnO/WO_3 nano-composite films deposited on ITO- and FTO-coated glass substrates

Other important optical features of the nano-composite films such as transmittance difference (T) and photopic contrast ratio (PCR) values at coloration and bleaching stages can be driven using:

$$\Delta T = T_c - T_b \tag{3}$$

$$PCR = T_b/T_c \tag{4}$$

Moreover, the optical density (ΔOD) and coloration efficiency (CE) of the films are typically evaluated according to following formula's:

$$\Delta OD = \ln\left(T_b/T_c\right) \tag{5}$$

$$CE = \Delta OD/Q_{\text{in}} = \ln\left(T_b/T_c\right)/q/A \tag{6}$$

which T_b, T_c, Q_{in} and A are specified as bleaching, coloring transmittance, current value at the coloration stage and surface area of the nano-composite thin films, respectively. The entire calculated values are listed in Table 4. The bleaching, coloring and transmittance differences versus wavelength curves of the films are illustrated in Fig. 8b–d.

According to the CE results, the highest values achieved for films coated onto FTO-coated glass substrates at the given wavelength. It was suggested that the highest values of CE contributed to the highest RMS roughness values as well as indium doping in the films coated upon FTO-coated glass substrate compared to ITO-coated glass substrate. The obtained coloration efficiency values of our produced nano-composite thin films are higher than maximum CE values recently shown in the literature by Wei (78.5 cm^2/C) [46], Shi (16.5 cm^2/C) [47] et al., for undoped ZnO in addition to works ascertained via Wang (46.64 cm^2/C) [48] and Bi (69 cm^2/C) [49] et al., for doped ZnO materials. Moreover, in this research, the results found for CE are greater than newly published by Yang (70.6 cm^2/C) [50] et al., for WO_3/ZnO core–shell nano-rod as well. By comparing the Yang's results, it explicitly seems our findings have proved improving coloration efficiency of the ZnO films by indium cooperation.

In Table 5, accumulated charges were measured and given in the following table for intercalation/deintercalation process of the electrochromic cell.

Table 5 Measured accumulated charge in intercalation/deintercalation process for the cells

	Value	Unit	Sign
In-doped ZnO/WO_3/ITO-coated glass			
0–100 secs	2.92	mA.s	Positive
100–200 secs	10.2	mA.s	Negative
In-doped ZnO/WO_3/FTO-coated glass			
0–100 secs	3.55	mA.s	Positive
100–200 secs	13.62	mA.s	Negative

4 Conclusion

The indium-doped ZnO/WO_3 nano-composites were successfully deposited on the un-coated, ITO-coated and FTO-coated glass substrates using thermionic vacuum arc technique. The surface results, the smoother surface observed for films coated onto glass substrate proved that results are obtained by field emission scanning electron microscopy images and thickness. The optical band values of the thin films were changed and relied upon indium concentration. The structural properties confirm formation of wurtzite ZnO structure upon 3 selected substrates. Based on EC examinations, higher resistance had observed for films deposited on ITO-coated glass substrate compared to FTO-coated glass substrate due to roughness values as well as indium contribution. Comparatively, the faster ion transfer occurred for films on ITO-coated glass substrate because of roughness and structure differences by means of the chronoamperometry results. Absence of

Table 4 The calculated electrochromic performance of the nano-composite thin films

Q_{in}	Q_{din}	Reversibility	Sample	Transmittance		ΔOD	CE	Wavelength
(mC/cm^2)		%		% T_b	% T_c	%	(cm^2/C)	(nm)
10.22	2.97	30	In-doped ZnO/WO_3 deposited onto ITO-coated glass	47	35	12	29	550
10.22	2.97	30		53	33	20	46	632
5.5	2.74	50	In-doped ZnO/WO_3 deposited onto FTO-coated glass	17	12	37	69	550
5.5	2.74	50		18	12	43	80	632

current decay in the both coloration and bleaching stages has proved superiority and stability of the films as well as indium influence which is an advantage of our coating technique. The highest reversibility and coloration efficiency of the In-doped ZnO/WO_3 films are achieved upon FTO-coated glass substrates by 50% and 80 cm^2/C at 632 nm, respectively.

Acknowledgements This research activity was supported as Eskişehir Osmangazi University Scientific Research Council, and Grants Number is 201719041.

Compliance with ethical Standards

Conflict of interest The authors declare that there is no conflict of interest.

References

1. Cai G et al (2015) Electrochromo-supercapacitor based on direct growth of NiO nanoparticles. Nano Energy 12:258–267
2. Zhou D et al (2016) Bi-functional Mo-doped WO3 nanowire array electrochromism-plus electrochemical energy storage. J Colloid Interface Sci 465:112–120
3. Lam S-M et al (2013) Investigation on visible-light photocatalytic degradation of 2, 4-dichlorophenoxyacetic acid in the presence of MoO3/ZnO nanorod composites. J Mol Catal A: Chem 370:123–131
4. Mohammadigharehbagh R et al (2018) Investigation of the optical properties of the indium-doped ZnO thin films deposited by a thermionic vacuum arc. Optik 157:667–674
5. Wei D et al (2012) A nanostructured electrochromic supercapacitor. Nano Lett 12(4):1857–1862
6. Baetens R, Jelle BP, Gustavsen A (2010) Properties, requirements and possibilities of smart windows for dynamic daylight and solar energy control in buildings: A state-of-the-art review. Sol Energy Mater Sol Cells 94(2):87–105
7. Akkurt N et al (2019) Electrochromic properties of UV-colored WO 3 thin film deposited by thermionic vacuum arc. J Mater Sci: Mater in Electron. 31(2):1293–1301
8. Buch VR, Chawla AK, Rawal SK (2016) Review on electrochromic property for WO3 thin films using different deposition techniques. Mater Today: Proc 3(6):1429–1437
9. Hunge Y et al (2016) Visible light catalysis of methyl orange using nanostructured WO3 thin films. Ceram Int 42(1):789–798
10. Mohammadigharehbagh R et al (2018) The investigation of the Cr doped ZnO thin films deposited by thermionic vacuum arc technique. Mater Res Express 5(2):026403
11. Park H et al (2017) A skin-integrated transparent and stretchable strain sensor with interactive color-changing electrochromic displays. Nanoscale 9(22):7631–7640
12. Li B, Shao X, Liu T, Shao L, Zhang B (2016) Construction of metal/WO2. 72/rGO ternary nanocomposites with optimized adsorption, photocatalytic and photoelectrochemical properties. Appl Catal B 198:325–333
13. Girtan M et al (2010) On the structural, morphological, optical and electrical properties of sol-gel deposited ZnO: In films. Thin Solid Films 519(2):573–577
14. Kim MS et al (2012) Growth and characterization of indium-doped zinc oxide thin films prepared by sol-gel method. Acta Phys Pol-Ser A Gener Phys 121(1):217
15. Gupta RK, Shridhar N, Katiyar M (2002) Structure of ZnO films prepared by oxidation of metallic zinc. Mater Sci Semicond Process 5(1):11–15
16. Benouis C et al (2010) The effect of indium doping on structural, electrical conductivity, photoconductivity and density of states properties of ZnO films. J Alloy Compd 490(1–2):62–67
17. Lin D et al (2009) Enhanced photocatalysis of electrospun Ag–ZnO heterostructured nanofibers. Chem Mater 21(15):3479–3484
18. Coman T et al (2017) Sequential PLD in oxygen/argon gas mixture of Al-doped ZnO thin films with improved electrical and optical properties. Appl Surf Sci 418:456–462
19. Teke A et al (2004) Excitonic fine structure and recombination dynamics in single-crystalline ZnO. Phys Rev B 70(19):195207
20. Sandeep K, Bhat S, Dharmaprakash S (2017) Structural, optical, and LED characteristics of ZnO and Al doped ZnO thin films. J Phys Chem Solids 104:36–44
21. Rajalakshmi R, Angappane S (2013) Synthesis, characterization and photoresponse study of undoped and transition metal (Co, Ni, Mn) doped ZnO thin films. Mater Sci Eng: B 178(16):1068–1075
22. Ghosh S, Bhaktha BS (2017) Heat-treatment controlled structural and optical properties of sol-gel fabricated Eu: ZnO thin films. Opt Mater 64:288–294
23. Zhang W et al (2013) Structural, optical and magnetic properties of Zn1–xFexO powders by sol-gel method. Appl Surf Sci 284:49–52
24. Mickan M et al (2017) Restoring the properties of transparent Al-doped ZnO thin film electrodes exposed to ambient air. J Phys Chem C 121(27):14426–14433
25. Onofre Y, de Castro S, de Godoy M (2017) Effect of traps localization in ZnO thin films by photoluminescence spectroscopy. Mater Lett 188:37–40
26. Lv J et al (2012) Effect of solution concentrations on crystal structure, surface topographies and photoluminescence properties of ZnO thin films. Superlattices Microstruct 51(6):886–892
27. Trandafilović LV et al (2012) Fabrication and antibacterial properties of ZnO–alginate nanocomposites. Carbohydr Polym 88(1):263–269
28. Børseth TM, Svensson BG, Kuznetsov AY, Klason P, Zhao QX, Willander M (2006) Identification of oxygen and zinc vacancy optical signals in ZnO. Appl Phys Lett. 89(26):262112
29. Ariyakkani P, Suganya L, Sundaresan B (2017) Investigation of the structural, optical and magnetic properties of Fe doped ZnO thin films coated on glass by sol-gel spin coating method. J Alloy Compd 695:3467–3475
30. Chandrinou C et al (2009) PL study of oxygen defect formation in ZnO nanorods. Microelectron J 40(2):296–298
31. Wang R, Xu G, Jin P (2004) Size dependence of electron–phonon coupling in ZnO nanowires. Phys Rev B 69(11):113303
32. Ye F et al (2012) The field emission of indium-doped ZnO films fabricated by room temperature DC magnetron sputtering. Phys B 407(1):64–67
33. Escobedo-Morales A, Pal U (2011) Effect of In, Sb and Ga doping on the structure and vibrational modes of hydrothermally grown ZnO nanostructures. Curr Appl Phys 11(3):525–531
34. Cremonesi A et al (2008) Micro-raman spectroscopy on polyethylene-glycol assisted sol–gel meso and macroporous WO3 thin films for electrochromic applications. Thin Solid Films 516(12):4128–4132

35. Santato C et al (2001) Crystallographically oriented mesoporous WO3 films: synthesis, characterization, and applications. J Am Chem Soc 123(43):10639–10649
36. Milanova M et al (2011) Glass formation and structure of glasses in the ZnO–Bi2O3–WO3–MoO3 system. J Non-Cryst Solids 357(14):2713–2718
37. Alim KA, Fonoberov VA, Balandin AA (2005) Origin of the optical phonon frequency shifts in ZnO quantum dots. Appl Phys Lett 86(5):053103
38. Cuscó R et al (2007) Temperature dependence of raman scattering in ZnO. Phys Rev B 75(16):165202
39. Koutu V, Shastri L, Malik M (2016) Effect of NaOH concentration on optical properties of zinc oxide nanoparticles. Mater Sci-Pol 34(4):819–827
40. Errandonea D et al (2008) Combined raman scattering and ab initio investigation of pressure-induced structural phase transitions in the scintillator ZnWO4. Phys Rev B 78(5):054116
41. Manjón F et al (2005) Silent raman modes in zinc oxide and related nitrides. J Appl Phys 97(5):053516
42. Arguello C, Rousseau DL, Porto, SPdS (1969) First-order raman effect in wurtzite-type crystals. Phys Rev 181(3):1351
43. Zhao J et al (2010) Raman spectra and photoluminescence properties of In-doped ZnO nanostructures. Mater Lett 64(5):569–572
44. Xie Z et al (2018) Enhanced electrochromic performance of 2D grid-structured WO3 thin films. Thin Solid Films 653:188–193
45. Qin J et al (2011) Graphene-wrapped WO3 nanoparticles with improved performances in electrical conductivity and gas sensing properties. J Mater Chem 21(43):17167–17174
46. Wei W et al (2019) Three-Dimensional Structures of Nanoporous NiO/ZnO Nanoarray Films for Enhanced Electrochromic Performance. Chem-An Asian J 14(3):431–437
47. Shi J, Guo R, Yu S (2018) Electrochromic performance of Zn–Ti–O composite thin film with electrolyte dependence. J Solid State Electrochem 22(12):3815–3820
48. Wang M et al (2017) Influence of thickness on the structure, electrical, optical and electrochromic properties of AZO thin films and their inorganic all-solid-state devices. Electrochim Acta 258:1336–1347
49. Bi Z et al (2015) A novel nanocomposite of WO3 modified Al-doped ZnO nanowires with enhanced electrochromic performance. Mater Lett 160:186–189
50. Yang S-H, Tseng G-Y, Kao C-F (2019) Electron thermionic field emission and flow model of rapid-switching energy-saving electrochromic WO3/ZnO core-shell nanorod channels. J Electrochem Soc 166(2):H70–H76

Publisher's Note Springer Nature remains neutral with regard to jurisdictional claims in published maps and institutional affiliations.